CHAPTER 1

SOURCE-COUPLED CONVERTERS AND INPUT FILTER INTERACTION

The previous chapter investigated the performance of the converters coupled with a load subsystem, consisting of a filter stage and regulated converter. The load subsystem alters the converter performance but it usually does not destabilize or notably degrade the converter performance.

Now we study the impacts of the source subsystem on the converter performance. In contrast, the source subsystem could easily make the converter unstable or unsatisfactory. This chapter presents the dynamic analysis and preventive measures for such instability and performance degradation.

The source subsystem is a combination of the voltage source, filter stages, and converters, all located in the upstream side of the converter. The structure of the source subsystem is widely varied and complex. Even so, the impacts of all source subsystems can be described by the same equations, regardless of the difference in their structure and complexity.

In this chapter, we use a simple structure to study the impacts of source subsystems. The analysis will be done in a general manner so that the outcomes can be broadened to more complex cases. Such extensions will be presented in Part III of this book, which covers the stability and performance of general dc power conversion systems.

1.1 INPUT FILTER-COUPLED CONVERTER AND INPUT FILTER INTERACTION

A converter powered from a practical source subsystem, yet loaded with an ideal current sink, is denoted as the *source-coupled converter*. The converter directly connected to the voltage source is referred to as the uncoupled converter in this chapter.

All source-coupled converters can be represented by the block diagram shown in Fig. 1.1, where the source subsystem is replaced by Thevenin's form. In Fig. 1.1, v_S is the open-circuit voltage of the source subsystem and $Z_s(s)$ is the source impedance seen by the converter. The source impedance $Z_s(s)$ corresponds to the output impedance of the source subsystem. Once the characteristics of $Z_s(s)$ are known, we can analyze all the the source-coupled converters in a unified manner.

1.1.1 Input Filter-Coupled Converters

Figure 1.2 shows a simple source-coupled converter. Here, the source subsystem consists of an ideal voltage source and single-stage filter. The filter stage in front of the converter is called an *input filter*. The converter coupled with an input filter is denoted as the *input filter-coupled converter*. The impacts of an input filter on the downstream converter are referred to as the *input filter interaction*.

All converters for practical applications should meet compulsory EMI standards. An input filter stage is necessary for converters to comply with the EMI standards [1]. Thus, all practical converters are exposed to the potential performance degradation or even instability, due to the detrimental input filter interaction.

The input filter is usually treated as a part of the converter stage. The input filter and converter are thus designed together as one functional unit. The design process should consider the impacts of input filter for stability and performance of the input filter-coupled converter.

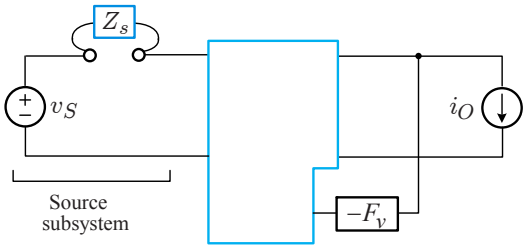

Figure 1.1 Block diagram of source-coupled converter.

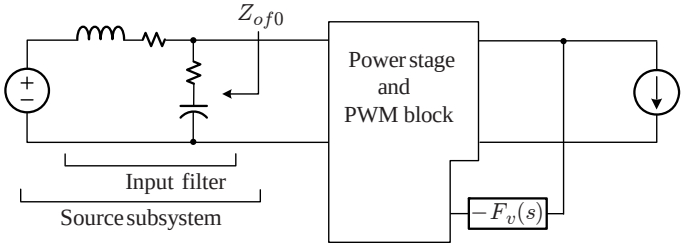

Figure 1.2 Input-filter coupled converter.

1.1.2 Transfer Functions of Input Filter-Coupled Converter

Using Thevenin's theorem, The input filter-coupled converter in Fig. 1.2 is modified into Fig. 1.3. The Z_{of0} in Fig. 1.3 is the output impedance of the input filter, which functions as the source impedance of the converter. The detailed analysis of Fig. 1.3 using the Middlebrook's EET was covered in Chapter 5 and the results are summarized in Table **??**.

Referring to Table **??**, the audio-susceptibility of the input filter-coupled converter, $A_{uS}(s)$, is given by

$$A_{uS}(s) = A_{uf}(s)\, A_{uU}(s)\, \frac{1}{1 + \dfrac{Z_{of0}}{Z_{iU}(s)}} \tag{1.1}$$

where $A_{uf}(s)$ is the input-to-output transfer function of the input filter, $A_{uU}(s)$ is the audio-susceptibility, and $Z_{iU}(s)$ is the input impedance of the uncoupled converter.

The output impedance of the input filter-coupled converter, $Z_{oS}(s)$, is expressed as

$$Z_{oS}(s) = Z_{oU}(s)\, \frac{1 + \dfrac{Z_{of0}}{Z_i'(s)}}{1 + \dfrac{Z_{of0}}{Z_{iU}(s)}} \tag{1.2}$$

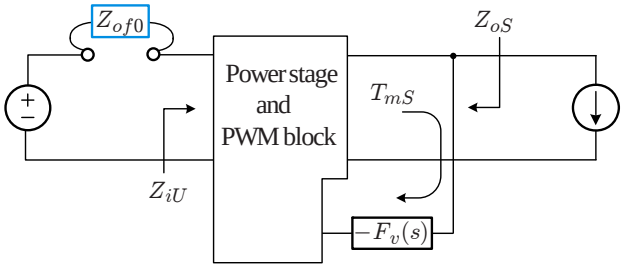

Figure 1.3 Block diagram of input filter-coupled converter.

where $Z_{oU}(s)$ is the output impedance of the uncoupled converter and $Z_i'(s)$ is the input impedance of the uncoupled converter, evaluated with the voltage feedback disconnected and output port shorted. This impedance is referred to as the *open-loop output-shorted input impedance*.

The loop gain of the input filter-coupled converter, $T_{mS}(s)$, is given by

$$T_{mS}(s) = T_{mU}(s) \frac{1 + \dfrac{Z_{of0}}{Z_i''(s)}}{1 + \dfrac{Z_{of0}}{Z_i'''(s)}} \tag{1.3}$$

where $T_{mU}(s)$ is the loop gain of the uncoupled converter. The $Z_i''(s)$ is the closed-loop input impedance of the uncoupled converter, determined with the output voltage nullified. This impedance is called the *output-nullified input impedance*. The $Z_i'''(s)$ is the input impedance, assessed with the output feedback disconnected. This impedance is termed as the *open-loop input impedance*.

The impacts of the input filter, or more precisely the impact of the filter output impedance Z_{of0}, are now analyzed using the expressions (1.1), (1.2), and (1.3). The critical factors in such analyses are the various input impedances of the converter, defined with the different operational conditions.

- $Z_{iU}(s)$: the closed-loop input impedance
- $Z_i'(s)$: the open-loop output-shorted input impedance
- $Z_i''(s)$: the output-nullified input impedance
- $Z_i'''(s)$: the open-loop input impedance

Figure 1.4 shows the circuit representations of the four input impedances of the uncoupled converter. Evaluations of these input impedances will be discussed later as they emerge in analyses. Readers are encouraged to refer to Section 3.5.2 for the theoretical details behind the current section.

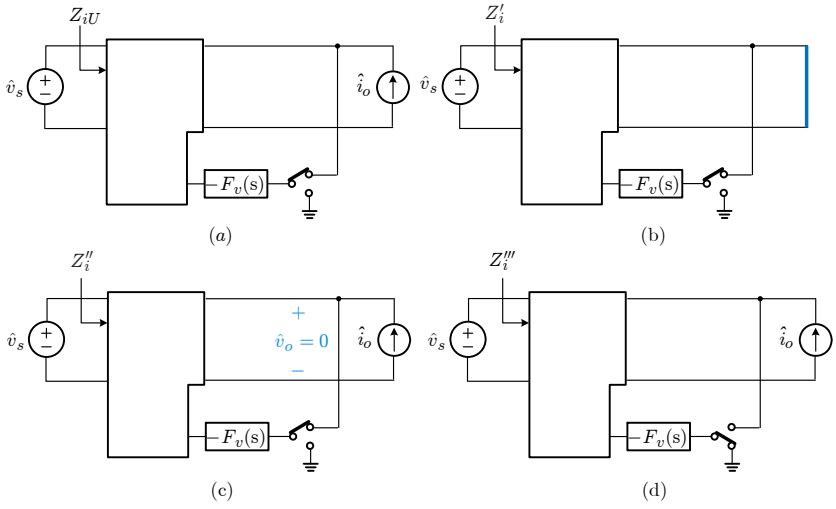

Figure 1.4 Four input impedances of uncoupled converter. (a) Closed-loop input impedance, Z_{iU}. (b) Open-loop output-shorted input impedance, Z_i'. (c) Output nullified input impedance, Z_i''. (d) Open-loop input impedance, Z_i'''.

1.1.3 Condition for Stability

The stability of the source-coupled converter can be assessed using the loop gain expression (1.3). The characteristic equation of the source-coupled converter is given by

$$1 + T_{mS}(s) = 0 \quad \Rightarrow \quad 1 + T_{mU}(s)\,\frac{1 + \dfrac{Z_{of0}}{Z_i''(s)}}{1 + \dfrac{Z_{of0}}{Z_i'''(s)}} = 0 \tag{1.4}$$

This expression is converted into

$$1 + \frac{Z_{of0}}{Z_i'''(s)} + T_{mU}(s)\Big(1 + \frac{Z_{of0}}{Z_i''(s)}\Big) = 0 \tag{1.5}$$

and rearranged

$$\big(1 + T_{mU}(s)\big)\Big(1 + \frac{Z_{of0}}{Z_i'''(s)}\frac{1}{1 + T_{mU}(s)} + \frac{Z_{of0}}{Z_i''(s)}\frac{T_{mU}(s)}{1 + T_{mU}(s)}\Big) = 0 \tag{1.6}$$

The above equation can be written in a compact form using the expression for the input impedance, $Z_{iU}(s)$, of the uncoupled-converter. The $Z_{iU}(s)$ was found as

$$\frac{1}{Z_{iU}(s)} = \frac{1}{Z_i'''(s)}\frac{1}{1 + T_{mU}(s)} + \frac{1}{Z_i''(s)}\frac{T_{mU}(s)}{1 + T_{mU}(s)} \tag{1.7}$$

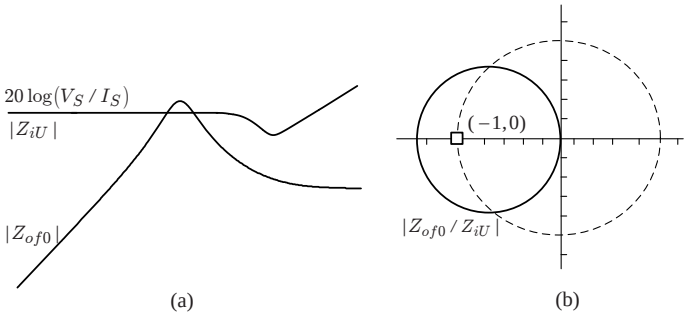

Figure 1.5 Instability due to input filter interaction (a) Overlap between $|Z_{of0}|$ and $|Z_{iU}|$. (b) Polar plot of Z_{of0}/Z_{iU}.

in Section 5.3.3 based on Middlebrook's feedback theorem. From (1.6) and (1.7), the final expression for the characteristic equation becomes

$$\big(1+T_{mU}(s)\big)\Big(1+\frac{Z_{of0}}{Z_{iU}(s)}\Big)=0 \tag{1.8}$$

The expression (1.8) reveals that the poles of the source-coupled converter are the union of the poles of the uncoupled converter and the solutions of $1+Z_{of0}/Z_{iU}(s)=0$. This implies that the roots of $1+Z_{of0}/Z_{iU}(s)=0$ become the additional poles of the input filter-coupled converter. Nyquist stability criterion can thus be applied to the impedance ratio $Z_{of0}/Z_{iU}(s)$ to test whether the input filter destabilizes the converter.

Figure 1.5 illustrates the instability caused by the input filter interaction. As briefly introduced earlier and will be elaborated later, $Z_{iU}(s)$ behaves as a negative resistance at low frequencies. The negative resistance is the prime cause of instability.

As shown in Fig. 1.5(a), the output impedance $|Z_{of0}|$ produces a peaking, yielding an overlap with $|Z_{iU}|$. For most input filters, the peaking occurs in the frequency range where $Z_{iU}(s)$ exhibits the negative resistance characteristics. During the overlap, the phase of the filter output impedance, $\angle Z_{of0}$, changes from $+90^\circ$ to -90°, while the phase of the converter's input impedance, $\angle Z_{iU}$, remains at -180°. Thus, the phase of the impedance ratio $Z_{of0}/Z_{iU}(s)$ varies as

$$90^\circ-(-180^\circ)>\angle\left(Z_{of0}/Z_{iU}\right)>-90^\circ-(-180^\circ)$$

$$\Rightarrow \quad 270^\circ>\angle\left(Z_{of0}/Z_{iU}\right)>90^\circ$$

Under this situation, the polar plot trajectory of $Z_{of0}/Z_{iU}(s)$ invariably encircles the $(-1,0)$ point, as illustrated in Fig. 1.5(b), and the converter becomes unstable. An example of this *input filter-induced instability* will be given shortly.

Instability will be prevented when the peak value of the filter output impedance $|Z_{of0}|_{peak}$ stays lower than the low-frequency asymptote of $|Z_{iU}(0)|$. This requirement ensures that the polar plot remains inside the unit circle, thereby precluding any chance of encircling the $(-1,0)$ point. It will be shown that the low-frequency

asymptote is given by $|Z_{iU}(0)| = 20\log(V_S/I_S)$, as shown in Fig. 1.5(a), where V_S is the dc voltage supplied to the converter and I_S is the dc current flowing into the converter. The stability condition now becomes

$$|Z_{of0}|_{peak} < 20\log\left(\frac{V_S}{I_S}\right) \tag{1.9}$$

This stability condition is valid for all converters regardless of the converter topologies and control schemes.

Input Filter-Induced Instability — EXAMPLE 1.1

This example illuminates an input filter-induced instability. A simplified circuit diagram of the input filter-coupled buck converter is shown in Fig. 1.6(a). The input filter parameters are chosen as $L_f = 160$ μH, $R_{lf} = 0.002\ \Omega$, $C_f = 160$ μF, and $R_{cf} = 0.002\ \Omega$. A current mode-controlled buck converter is power from a 15 V voltage source vis a single-stage input filter. The buck converter regulates the output voltage at $V_O = 5$ V. In order to demonstrate the input filter-induced instability, the output current of the buck converter is varied between $I_O = 1\text{ A} \Rightarrow 5\text{ A} \Rightarrow 1\text{ A}$. The frequency-domain dynamics and transient waveforms of the buck converter are shown in Figs. 1.6(b) through 1.6(d).

Figure 1.6(b) depicts the output impedance of the input filter, Z_{of0}, in comparison with the input impedances of the buck converter with two different output currents: $Z_{iU}(s)$ with $I_O = 1$ A and $Z'_{iU}(s)$ with $I_O = 5$ A. The low-frequency asymptotes of the input impedances are evaluated as

$$|Z_{iU}(0)| = 20\log\frac{V_S}{I_S} = 20\log\frac{V_S^2}{V_O I_O} = 20\log\frac{15^2}{5\cdot 1} = 26\text{ dB}$$

and

$$|Z'_{iU}(0)| = 20\log\frac{15^2}{5\cdot 5} = 6\text{ dB}$$

assuming a lossless operation for the buck converter.

With $I_O = 1$ A, $|Z_{iU}(0)|$ falls well below $|Z_{of0}|_{peak}$, thus meeting the stability requirement. When the output current is increased to $I_O = 5$ A, $|Z'_{iU}(0)|$ drops by 20 dB and falls below $|Z_{of0}|_{peak}$ around the resonant frequency of the input filter

$$\omega_o = \frac{1}{\sqrt{L_f C_f}} = \frac{1}{\sqrt{240\times 10^{-6}120\times 10^{-6}}} = 2\pi\cdot 220\text{ Hz} \tag{1.10}$$

Figure 1.6(c) displays the polar plot trajectories for the impedance ratios of $Z_{of0}/Z_{iU}(s)$ with $I_O = 1$ A and $Z_{of0}/Z'_{iU}(s)$ with $I_O = 5$ A. The polar plot of $Z_{of0}/Z_{iU}(s)$ stays inside the unit circle. With the increased output current, the polar plot of $Z_{of0}/Z'_{iU}(s)$ encircles the $(-1, 0)$ point and predicts instability.

Figure 1.6(d) exhibits the output current i_O, input voltage v_S, and output voltage v_O of the buck converter. The converter initially shows very stable waveforms with $I_O = 1$ A. When the output current is stepped up to $I_O = 5$ A, the input voltage initiates an unstable oscillation at $\omega_o = 1/\sqrt{L_f C_F} = 2\pi\cdot 220$ Hz. When I_O is reduced to 1 A, the converter returns the stable operation.

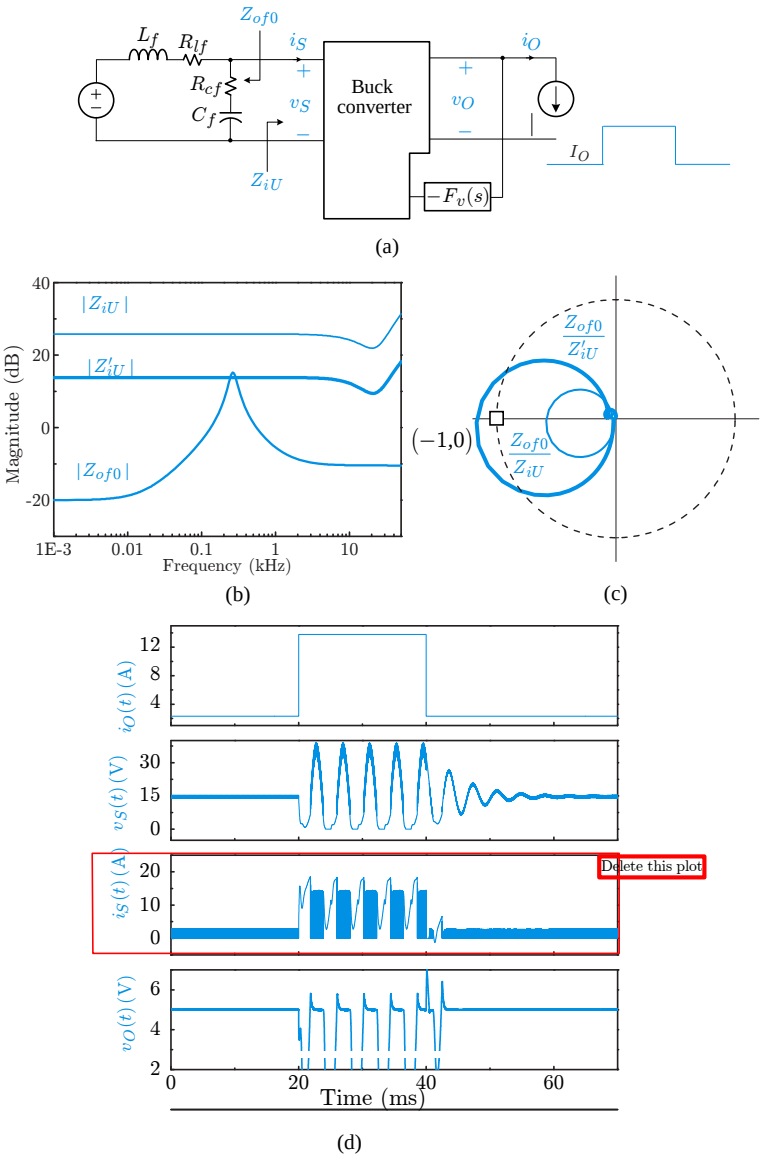

Figure 1.6 Input filter-induced instability. (a) Input filter coupled buck converter. (b) Bode plot of filter output impedance Z_{of0} and converter input impedance Z_{iU}. (c) Polar plot trajectory of impedance ratio Z_{of0}/Z_{iU}. (d) Circuit waveforms.

As demonstrated in this example, the stability requirement of $|Z_{of0}|_{peak} < 20\log(V_S/I_S)$ should be meet at the maximum value of I_S.

1.1.4 Conditions for Minimal Input Filter Interaction

The conditions for the minimal input filter interaction are readily seen from the expressions of the converter performance. The output impedance of the input filter coupled converter is expressed as

$$Z_{oS}(s) = Z_{oU}(s)\,\frac{1+\dfrac{Z_{of0}}{Z_i'(s)}}{1+\dfrac{Z_{of0}}{Z_{iU}(s)}}$$

It is evident that the output impedance does not change if the conditions $|Z_{of0}/Z_{iU}| \ll 1$ and $|Z_{of0}/Z_i'| \ll 1$ are met for all frequencies.

The loop gain of the input filter-coupled converter is given by

$$T_{mS}(s) = T_{mU}(s)\,\frac{1+\dfrac{Z_{of0}}{Z_i''(s)}}{1+\dfrac{Z_{of0}}{Z_i'''(s)}}$$

The loop gain of the input filter-coupled converter remains unaffected if the conditions $|Z_{of0}/Z_i''| \ll 1$ and $|Z_{of0}/Z_i'''| \ll 1$ are satisfied.

1.1.5 Performance Analysis under Input Filter Interaction

For any input filter design, the stability requirement of (1.9) must be met. However, it is not always possible to satisfy the conditions for minimal performance change, $|Z_{of0}/Z_{iU}| \ll 1$, $|Z_{of0}/Z_i'| \ll 1$, $|Z_{of0}/Z_i''| \ll 1$, and $|Z_{of0}/Z_i'''| \ll 1$. For such cases, the performance will be affected by the addition of an input filter even though the converter stays stable.

The performance of input filter-coupled converters can be analyzed from the expressions of (1.1) through (1.3). In this analysis, the roles of the various input impedances of the converter, $Z_{iU}(s)$, $Z_i'(s)$, $Z_i''(s)$, and $Z_i'''(s)$, are critical. The properties of the input impedances strongly depend on the control method and converter topology. Thus, the input filter interaction will develop very differently for various converter topologies and control methods. We proceed with the performance analysis of input filter-coupled converters using the following three illustrative cases.

- Case One: Boost converter with voltage mode control
- Case Two: Boost converter with current mode control
- Case Three: Buck converter with current mode control

These examples will demonstrate all the details about the input filter interaction and uncover the theories behind intricate behaviors of input filter-coupled converters. We will show that most input filter interactions will follow the pattern of one specific case among the above three cases. In other words, the three examples cover nearly all the possible instances of practical input filter interactions.

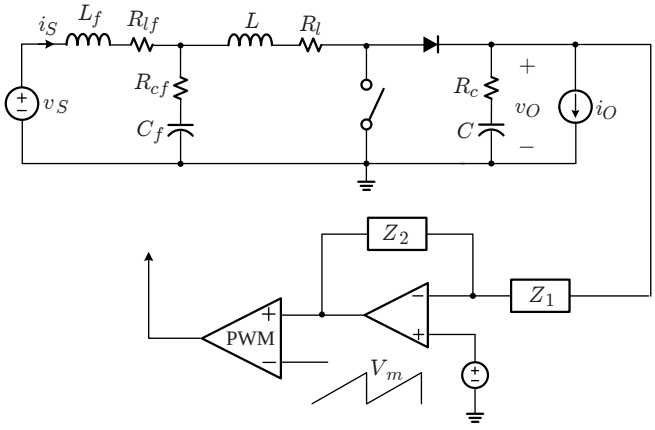

Figure 1.7 Input filter-coupled boost converter with voltage mode control.

1.2 INPUT FILTER INTERACTION CASE ONE – BOOST CONVERTER WITH VOLTAGE MODE CONTROL

As the first illustration, this section investigates the dynamics and performance of a boost converter employing voltage mode control.† Figure 1.7 depicts the boost converter considered in this section. The converter is powered from a voltage source v_S via a single-stage input filter and loaded with an ideal current sink. The boost converter operates with $V_S = 24$ V, $V_O = 46$ V, $I_O = 2$ A, $L = 160$ μH, $R_l = 0.045$ Ω, $C = 400$ μF, $R_c = 0.05$ Ω, $f_s = 50$ kHz, and $V_m = 1.8$ V. The three-pole two-zero circuit

$$F_v(s) = \frac{Z_2(s)}{Z_1(s)} = \frac{400}{s} \frac{\left(1 + \dfrac{s}{2\pi \cdot 207}\right)\left(1 + \dfrac{s}{2\pi \cdot 716}\right)}{\left(1 + \dfrac{s}{2\pi \cdot 6.20 \times 10^3}\right)\left(1 + \dfrac{s}{2\pi \cdot 7.96 \times 10^3}\right)}$$

is used for the voltage feedback compensation.

This section analyzes the influence of the input filter on the performance of the boost converter. The first step is to study the input impedances of the boost converter.

1.2.1 Input Impedance Analysis

The four different input impedances are involved with the input filter interaction. Each input impedance is defined under the specific operational condition, as discussed in the previous section. The circuit representation of the input impedances were shown in Fig. 1.4.

†Voltage mode control is rarely used for boost converters. However, this section considers voltage mode control because the characteristic features of the input filter interaction are well pronounced in this case.

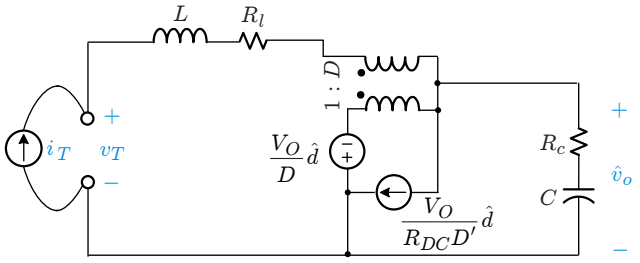

Figure 1.8 Small-signal model for input impedance analysis.

Figure 1.8 is the small-signal model of the boost converter, arranged for the input impedance evaluation. The four input impedances can be derived from Fig. 1.8 according to their respective definition. Derivations of such impedances will be covered later.

Using the outcomes of the upcoming analysis, Fig. 1.9(a) portrays the asymptotic plots for the four input impedances of the boost converter. Each impedance shows a very different evolution pattern. The impacts of the four input impedances are quite distinctive, as will be shown in the following analysis.

Among the four impedances, the closed-loop input impedance $Z_{iU}(s)$ is most influential because it determines stability of the converter. The closed-loop input impedance $Z_{iU}(s)$ is separately displayed in Fig. 1.9(b). Very importantly, it shows that $|Z_{iU}| = 20\log(V_S/I_S)$ and $\angle Z_{iU} = -180°$ at low frequencies. This implies the input impedance $Z_{iU}(s)$ behaves as a negative resistance of $-V_S/I_S$ at low frequencies. The negative resistance will be shown to prevail at the frequencies below the crossover frequency of the converter loop gain, ω_c in Fig. 1.9. The input impedance goes through a transitional dip over the crossover frequency ω_c and linearly increases at high frequencies. These characteristics were used in Section 7.1.3 to depict the input impedance of the uncoupled converter in Fig. 1.5.

Derivation of Input Impedances

This section deals with the derivations of the four input impedances of the boost converter. Referring to Fig. 1.8, the output-shorted open-loop input impedance is determined as

$$Z_i'(s) = \frac{v_T}{i_T}_{\hat{d}=0\ R_c+\frac{1}{sC}=0} = sL + R_l = \boxed{R_l\left(1+\frac{s}{\omega_z'}\right)} \tag{1.11}$$

with

$$\omega_z' = \frac{R_l}{L}$$

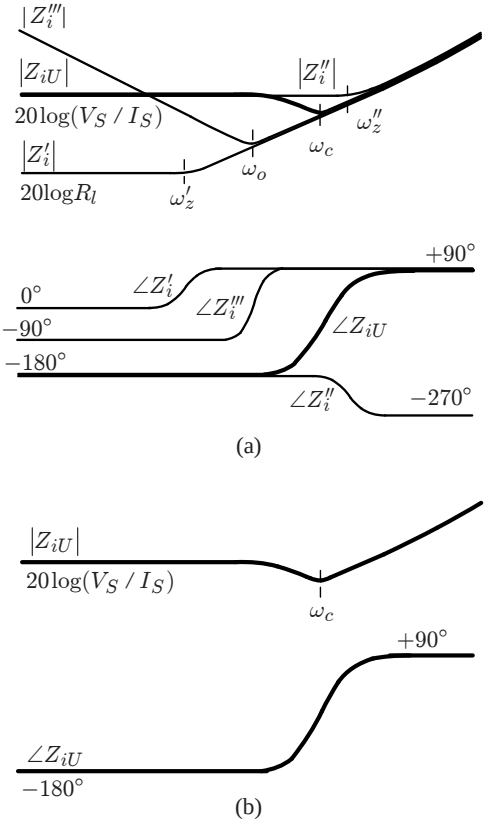

Figure 1.9 Asymptotic plots for input impedances. (a) Four input impedances. The definitions/expressions for the corner frequencies, ω_z', ω_o, ω_c, and ω_z'' are given in the ensuing section. (b) Input impedance Z_{iU}.

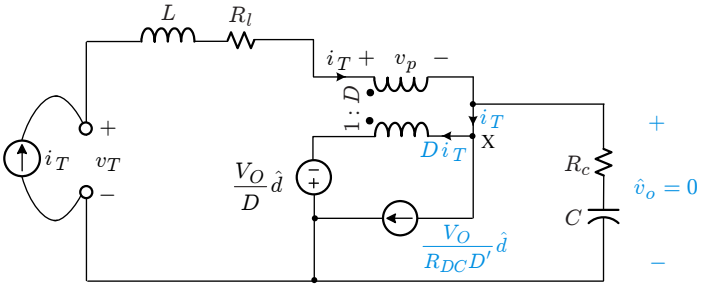

Figure 1.10 Small-signal model for evaluation of output-nullified input impedance.

The open-loop input impedance is given by

$$Z_i'''(s) = \frac{v_T}{i_T}_{\hat{d}=0} = sL + R_l + D'^2\left(R_c + \frac{1}{sC}\right) = \boxed{\frac{1 + \frac{s}{Q\omega_o} + \frac{s^2}{\omega_o^2}}{s\frac{C}{D'^2}}} \tag{1.12}$$

with

$$\omega_o = D'\sqrt{\frac{1}{LC}}$$

$$Q = \frac{1}{R_l + D'^2 R_c}\sqrt{\frac{L}{C}}$$

Figure 1.10 is the small-signal model of the power stage, modified to evaluate the output-nullified input impedance, $Z_i''(s)$. Referring to Fig. 1.10, the current source i_T is expressed as

$$i_T = Di_T + \frac{V_O}{R_{DC}D'}\hat{d} \tag{1.13}$$

and the input voltage is given by

$$v_T = (sL + R_l)i_T - V_O\hat{d} \tag{1.14}$$

From (1.13) and (1.14), it follows that

$$v_T = (sL + R_l)i_T - D'^2 R_{DC} i_T \tag{1.15}$$

yielding the expression for $Z_i''(s)$

$$Z_i''(s) = \frac{v_T}{i_T}_{\hat{d}\neq 0\,\hat{v}_o=0} = sL + R_l - D'^2 R_{DC} = \boxed{-k''\left(1 - \frac{s}{\omega_z''}\right)} \tag{1.16}$$

with

$$\omega_z'' = \frac{-R_l + D'^2 R_{DC}}{L} \approx \frac{D'^2 R_{DC}}{L}$$

The constant k'' in (1.16), which is the magnitude of the negative resistance, is evaluated as

$$k'' = D'^2 R_{DC} - R_l \approx D'^2 R_{DC} = D'^2\frac{V_O}{I_O} = \frac{D'V_O}{I_O/D'} = \frac{V_S}{I_S} \tag{1.17}$$

using the relationships $R_{DC} = V_O/I_O$ and $V_S/V_O = I_O/I_S = D'$ for the boost converter.

Now, we evaluate the closed-loop input impedance of the converter. As previously discussed, the input impedance of regulated converters is given by

$$\frac{1}{Z_{iU}(s)} = \frac{i_T(s)}{v_T(s)} = \frac{1}{Z_i''(s)}\frac{T_{mU}(s)}{1+T_{mU}(s)} + \frac{1}{Z_i'''(s)}\frac{1}{1+T_{mU}(s)} \tag{1.18}$$

where $T_{mU}(s)$ is the loop gain of the uncoupled converter. The above equation is approximated as

$$Z_{iU}(s) \approx \begin{cases} Z_i''(s) : \text{for frequencies below } T_{mU}(s) \text{ crossover frequency} \\ Z_i'''(s) : \text{for frequencies above } T_{mU}(s) \text{ crossover frequency} \end{cases} \tag{1.19}$$

The input impedance follows the output-nullified input impedance, $Z_i''(s)$, before the loop gain crossover frequency. In this frequency range, $Z_i''(s)$ holds the negative resistance characteristics. This confirms that the input impedance behaves as a negative resistance of $-V_S/I_S$ from the dc to the crossover frequency of the loop gain. At higher frequencies, the input impedance follows the open-loop input impedance, $Z_i'''(s)$, which is dominated by the power stage inductor.

The expressions of (1.11) through (1.16), along with relationship of (1.19), are used to construct the asymptotic plots in Fig. 1.9. Figure 1.11 shows the input impedances of the boost converter with the given operational conditions. The low-frequency asymptote of $|Z_{iU}|$ is evaluated as

$$\begin{aligned} |Z_{iU}(0)| = 20\log\left(\frac{V_S}{I_S}\right) &= 20\log\left(\frac{V_S}{V_O I_O/V_S}\right) = 20\log\left(\frac{V_S^2}{V_O I_O}\right) \\ &= 20\log\left(\frac{24^2}{46\cdot 2}\right) = 15.9 \text{ dB} \end{aligned} \tag{1.20}$$

Negative Input Resistance of Dc-to-Dc Converters

We verified that the input impedance of regulated converters behaves as a negative resistance, $-V_S/I_S$, at low frequencies. This unique property can also be concluded from the operational principle of the regulated converter.

The negative resistance is attributed to the fact that a regulated converter functions as a constant power load. Referring to Fig. 1.12(a), a regulated converter adjusts the duty ratio to maintain the output voltage constant, $v_O = V_O$, for a given load current I_O, even if the input voltage v_S changes. In other words, a regulated converter is a constant power load which always draws a predetermined power, $P = V_O I_O$. If the converter operates with a 100% efficiency, it follows

$$P = V_O I_O = v_S i_S \tag{1.21}$$

which indicates that

$$\frac{V_O}{v_S} = \frac{i_S}{I_O} = M \tag{1.22}$$

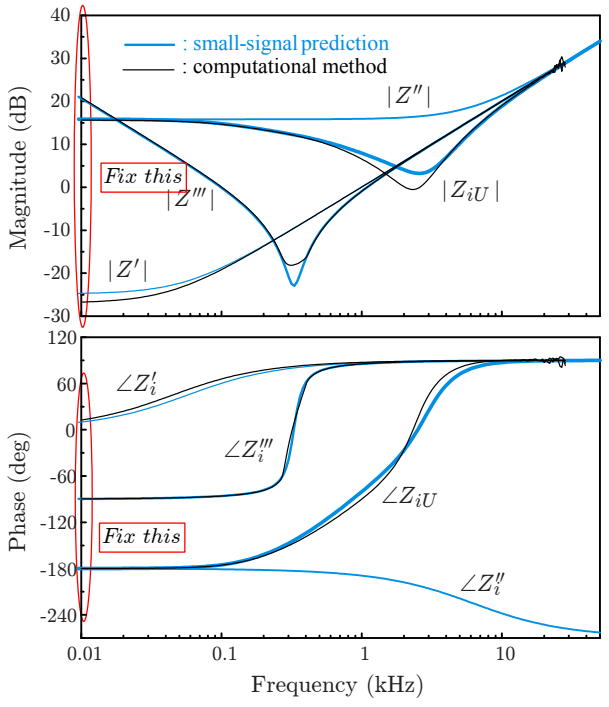

Figure 1.11 Input impedances of boost converter.

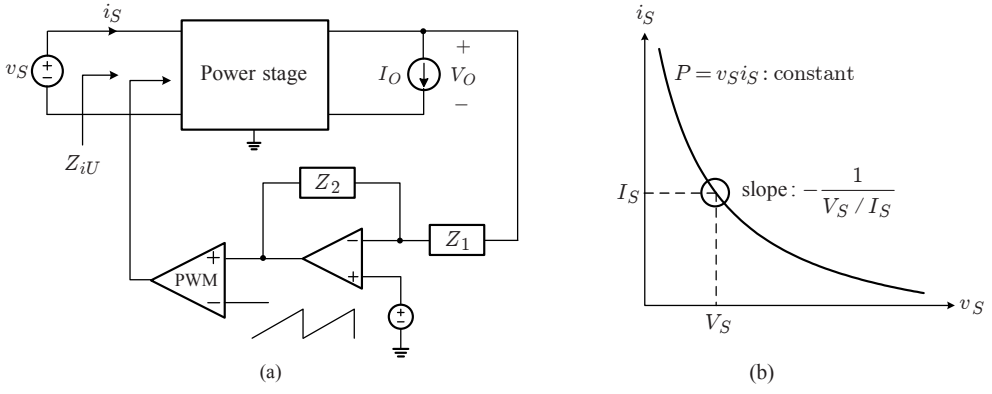

Figure 1.12 Negative input resistance of regulated dc-to-dc converter. (a) Block diagram. (b) $v_S - i_S$ plot.

where M denotes the forward voltage gain or reverse current gain. The input resistance of the converter is evaluated as

$$\frac{\mathrm{d}v_S}{\mathrm{d}i_S} = \frac{\mathrm{d}}{\mathrm{d}i_S}\left(\frac{P}{i_S}\right) = -\frac{P}{i_S^2} = -\frac{v_S}{i_S} = -\frac{1}{M^2}\frac{V_O}{I_O} = -\frac{1}{M^2}R_{DC} \tag{1.23}$$

where the facts $P = v_S i_S$, $v_S = V_O/M$, $i_S = MI_O$, and $R_{DC} = V_O/I_O$ are successively used. For the boost converter, the input resistance becomes $-D'^2 R_{DC}$. The input resistance $-D'^2 R_{DC}$ can be rewritten as $-V_S/I_S$, as shown in (1.17).

The negative input resistance is illustrated in Fig. 1.12(b) which depicts the v_S–i_S curve of a regulated converter. Because the product of v_S and i_S is a predetermined constant, $p = v_s\, i_S$, the slope of v_S–i_S curve is negative, as shown in Fig. 1.12(b). If v_S increases, i_S must decrease so that the input power $P = v_S\, i_S$ remains constant. The regulated dc-to-dc converter thus exhibits a negative incremental resistance, given by $-V_S/I_S$, at the operational point.

1.2.2 Stability Analysis

The circuit diagram of the boost converter is repeated in Fig. 1.13(a). The converter stability can be analyzed using the output impedance of the input filter, Z_{of0}, and the input impedance of the boost converter, $Z_{iU}(s)$. The converter becomes unstable when the polar plot of the impedance ratio $Z_{of0}/Z_{iU}(s)$ encircles the $(-1, 0)$ point.

Figure 1.13(b) shows $|Z_{iU}|$ of the boost converter and $|Z_{of0}|$ of the four different input filters, referred to as Filter A, B, C, and D.

- Filter A: $L_f = 21\ \mu$H, $R_{lf} = 0.04\ \Omega$, $C_f = 160\ \mu$F, $R_{cf} = 0.037\ \Omega$
- Filter B: $L_f = 140\ \mu$H, $R_{lf} = 0.05\ \Omega$, $C_f = 180\ \mu$F, $R_{cf} = 0.18\ \Omega$
- Filter C: $L_f = 610\ \mu$H, $R_{lf} = 0.125\ \Omega$, $C_f = 392\ \mu$F, $R_{cf} = 0.15\ \Omega$
- Filter D: $L_f = 2200\ \mu$H, $R_{lf} = 0.19\ \Omega$, $C_f = 1200\ \mu$F, $R_{cf} = 0.057\ \Omega$

All the four cases exhibit an impedance overlap and thus require the polar plot analysis. Fig. 1.13(c) shows the polar plot trajectories of $Z_{of0}/Z_{iU}(s)$ with the four different input filters. As the region of impedance overlap shifts from high frequencies to lower frequencies, from Filter A to Filter D, the circular-shaped trajectory rolls in the counter-clockwise direction. With Filter C and Filter D, the polar plot encircles the $(-1, 0)$ point, indicating the converter is unstable.

Instability occurs when $|Z_{of0}|$ overlaps with $|Z_{iU}|$ at low frequencies where $Z_{iU}(s)$ behaves as a negative resistance of $-V_S/I_S$. Conversely, the converter will remain stable provided that the impedance overlap at low frequency is avoided. This requirement is equivalent to $|Z_{of0}|_{peak} < 20\log(V_S/I_S)$, which is given in (1.9).

Figure 1.14 shows the loop gains of the boost converter combined with the four input filters, in parallel with the loop gain of the boost converter directly connected to the voltage source, $T_{mU}(s)$. Regarding the stability assessment, the loop gain provides the same information as the polar plot analysis. When Filter B is employed, the converter is barely stable with a small phase margin. With Filter C and Filter D, the converter becomes unstable with a negative phase margin.

Figure 1.15 exhibits the transient response of the converter due to the step load current changes of $I_O = 2\ \text{A} \Rightarrow 1\ \text{A} \Rightarrow 2\ \text{A}$. The output voltage is displayed with

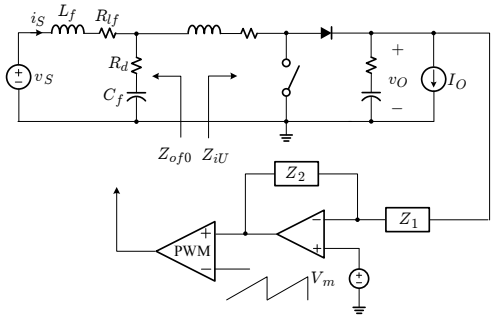

(a)

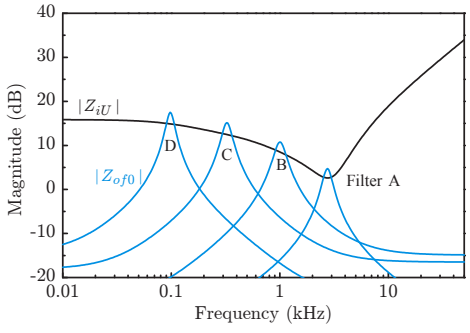

(b)

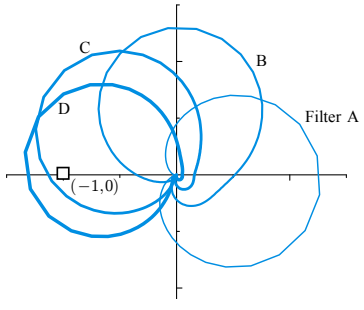

(c)

Figure 1.13 Stability analysis of boost converter. (a) Block diagram. (b) Bode plots of Z_{of0} and Z_{iU}. (c) Polar plot trajectories of Z_{of0}/Z_{iU}.

the different input filters, along with the case without any input filter. The output voltage becomes increasingly oscillatory until it exposes full instability with Filter C and Filter D.

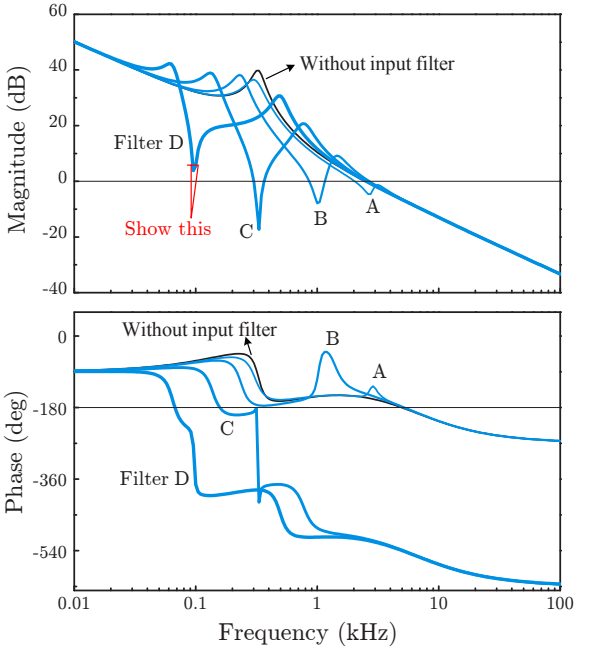

Figure 1.14 Loop gain of boost converter with different input filters.

1.2.3 Converter Performance Under Input Filter Interaction

The stability condition is $|Z_{of0}|_{peak} < V_S/I_S$, with the assumption that $|Z_{of0}|_{peak}$ occurs at the frequencies where $|Z_{iU}|$ stays on its low frequency asymptote. However, a more conservative guideline of $|Z_{of0}|_{peak} \ll V_S/I_S$ is frequently adopted. This guideline would offer stability despite certain drifts in the operational conditions of the converter and tolerances in the filter components.

The input filter design strategy of $|Z_{of0}|_{peak} \ll V_S/I_S$ is equivalent to maintaining the conditions $|Z_{of0}/Z_{iU}| \ll 1$ and $|Z_{of0}/Z_i''| \ll 1$ for all frequencies. These conditions are usually met when the input filters are properly designed. On the other hand, the other conditions for minimal input filter interaction, $|Z_{of0}/Z_i'| \ll 1$ and $|Z_{of0}/Z_i'''| \ll 1$, are often violated because they require an impractically large filter capacitor.

This section shows the closed-loop performance of the boost converter with an input filter of $L_f = 165\,\mu$H, $R_{lf} = 0.05\,\Omega$, $C_f = 1600\,\mu$F, and $R_{cf} = 0.13\,\Omega$. Unlike the input filters used for the stability analysis, this input filter is duly designed based on the standard design procedures [4]. Figure 1.16(a) shows the input impedances of the boost converter, in comparison with the output impedance of the input filter. The input filter meets only the conditions $|Z_{of0}/Z_{iU}| \ll 1$ and $|Z_{of0}/Z_i''| \ll 1$ for all frequencies, while not satisfying the conditions $|Z_{of0}/Z_i'| \ll 1$ and $|Z_{of0}/Z_i'''| \ll 1$

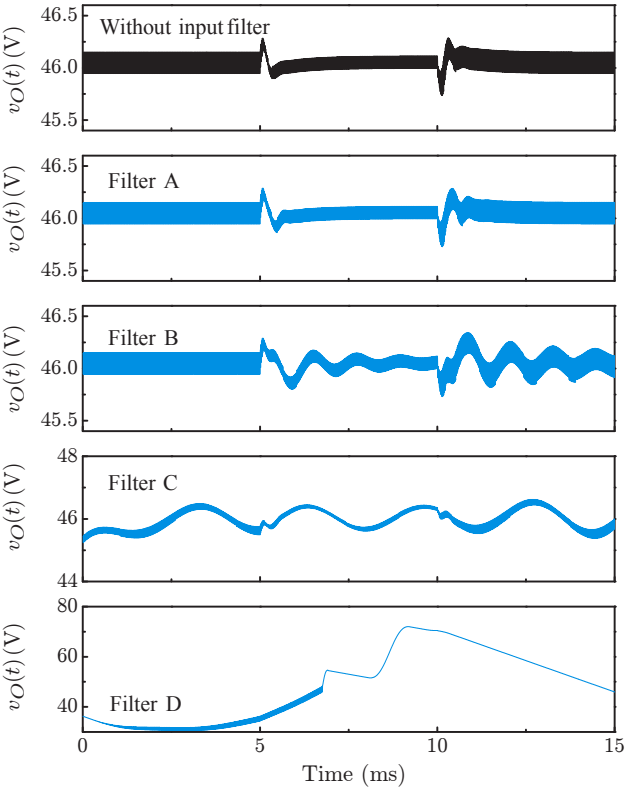

Figure 1.15 Step load current response of boost converter.

at certain frequencies. Thus, the converter will be stable but other performance will be affected.

The audio-susceptibility of the converter is simplified to

$$A_{uS}(s) = A_{uf}(s)A_{uU}(s)\,\frac{1}{1+\dfrac{Z_{of0}}{Z_{iU}(s)}} \approx A_{uf}(s)A_{uU}(s) \tag{1.24}$$

due to the prevailing condition of $|Z_{of0}/Z_{iU}| \ll 1$. Figure 1.16(b) shows the $|A_{uf}|$, $|A_{uU}|$, and $|A_{uS}|$. The input filter provides the additional attenuation, thus improving the noise immunity at high frequencies.

The output impedance is simplified into

$$Z_{oS}(s) = Z_{oU}(s)\,\frac{1+\dfrac{Z_{of0}}{Z_i'(s)}}{1+\dfrac{Z_{of0}}{Z_{iU}(s)}} \approx Z_{oU}(s)\left(1+\frac{Z_{of0}}{Z_i'(s)}\right) \tag{1.25}$$

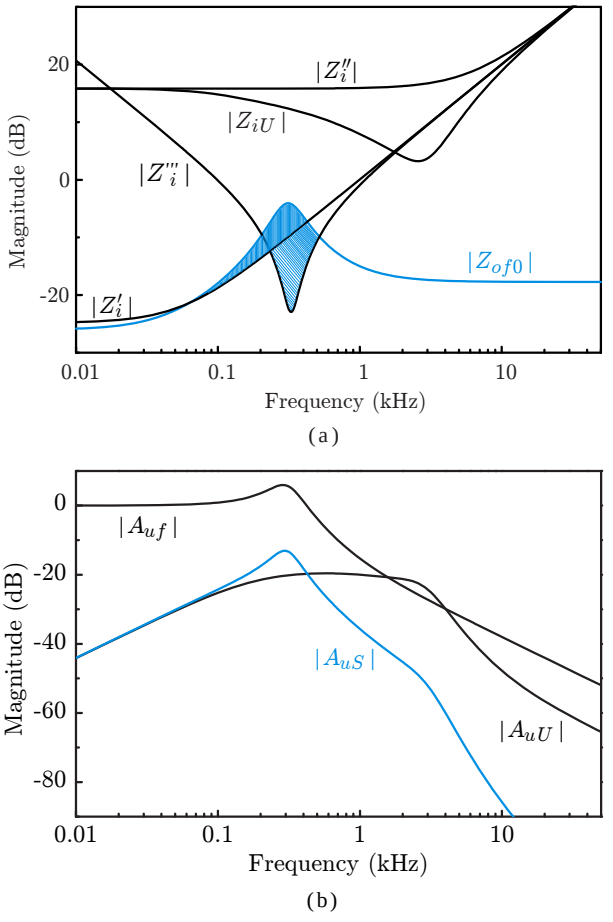

Figure 1.16 Transfer functions of boost converter with voltage mode control. (a) Converter input impedances and input filter output impedance. (b) Audio-susceptibility.

with the condition $|Z_{of0}/Z_{iU}| \ll 1$. This equation is further approximated as

$$\begin{aligned} Z_{oS}(s) &= Z_{oU}(s)\left(1+\frac{Z_{of0}}{Z_i'(s)}\right) \\ &\approx \begin{cases} Z_{oU}(s): & \text{where } |Z_{of0}/Z_i'| \ll 1 \\ Z_{oU}(s)\dfrac{Z_{of0}}{Z_i'(s)}: & \text{where } 1 \ll |Z_{of0}/Z_i'(s)| \end{cases} \end{aligned} \tag{1.26}$$

for the graphical analysis. Figure 1.17(a) shows the plots for $|Z_{oS}|$ and $|Z_{oU}|$ along with the impedance ratio $|Z_{of0}/Z_i'|$. As predicted from (1.26), $|Z_{oS}|$ exhibits an

increase from $|Z_{oU}|$ by the amount of $20\log|Z_{of0}/Z_i'|$ in the frequency range where $1 < |Z_{of0}/Z_i'|$ and an added boost at frequencies where $|Z_{of0}/Z_i'| \ll 1$ is not fully satisfied. However, the changes occur only at low frequencies, leaving the peak value and general shape of the output impedance unaltered. Thus, the step load response, which is closely related with the shape and parameters of the output impedance, will not be much affected.

The loop gain of the converter is approximated to

$$T_{mS}(s) = T_{mU}(s)\,\frac{1+\dfrac{Z_{of0}}{Z_i''(s)}}{1+\dfrac{Z_{of0}}{Z_i'''(s)}} \approx T_{mU}(s)\frac{1}{1+\dfrac{Z_{of0}}{Z_i'''(s)}} \tag{1.27}$$

with the condition $|Z_{of0}/Z_i''| \ll 1$. For the graphical analysis, this equation is transformed into

$$\begin{aligned} T_{mS}(s) &= T_{mU}(s)\frac{1}{1+\dfrac{Z_{of0}}{Z_i'''(s)}} \\ &\approx \begin{cases} T_{mU}(s) : \text{at frequencies where } |Z_{of0}/Z_i'''| \ll 1 \\ \dfrac{T_{mU}(s)}{\dfrac{Z_{of0}}{Z_i'''(s)}} : \text{at frequencies where } 1 \ll |Z_{of0}/Z_i'''| \end{cases} \end{aligned} \tag{1.28}$$

This analysis predicts a decrease in $|T_{mS}|$ by the amount of $20\log|Z_{of0}/Z_i'''|$ at frequencies where $1 < |Z_{of0}/Z_i'''|$. Figure 1.17(b) shows the loop gain of the converter along with the impedance ratio $|Z_{of0}/Z_i'''|$. The loop gain plots show a close agreement with the prediction of (1.28). The loop gain is only modified at mid frequencies and retains the high-frequency characteristics unchanged. In particular, the crossover frequency and stability margins remain essentially the same.

Figure 1.18 shows the transient response of the input filter-coupled boost converter, in parallel with that of the uncoupled converter. The output voltage and inductor current are shown in response to the step load changes of $I_O = 2\text{ A} \Rightarrow 1\text{ A} \Rightarrow 2\text{ A}$. This figure demonstrates that effects of the input filter on the transient response are indeed negligible, as predicted from the output impedance analysis.

1.3 INPUT FILTER INTERACTION CASE TWO – BOOST CONVERTER WITH CURRENT MODE CONTROL

The impacts of the input filter could emerge very differently, depending on the topologies and control methods of converters. Thus, the converter dynamics under the input filter interaction have long been studied by many researchers. In 1976, R. D. Middlebrook published a paper [5] dealing with the input filter interaction in a

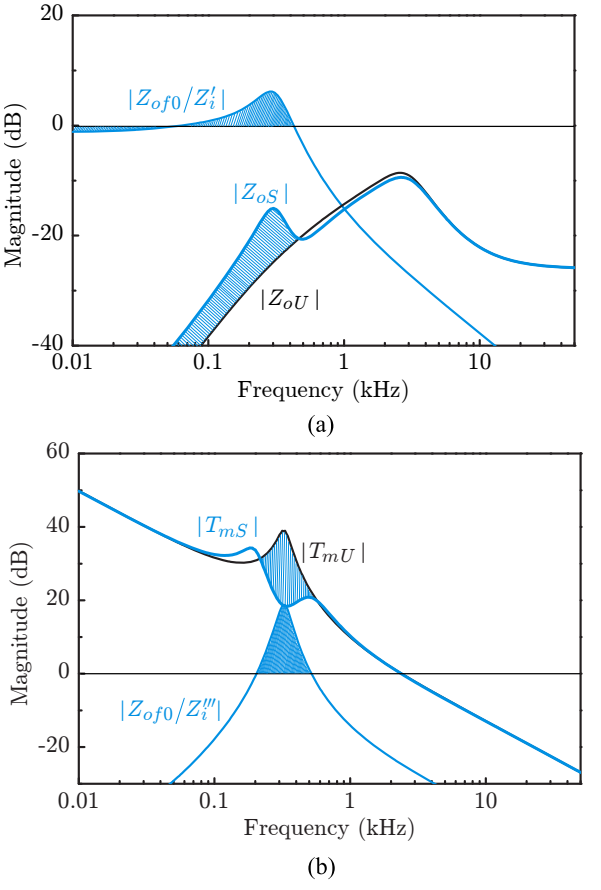

Figure 1.17 Transfer functions of boost converter with voltage mode control. (a) Output impedance. (b) Loop gain.

buck converter employing voltage mode control. As far as voltage mode control is considered, the conclusions of this study are expandable to the three basic converters. In the previous section, we investigated the effects of the input filter on the boost converter with voltage mode control.

Later publications [6,7] revealed that the input filter interaction in the current mode-controlled converters notably differs from the case of voltage mode control. Furthermore, the evolution and upshot of the input filter interaction widely vary with the converter topology. Indeed, the influence of the input filter cannot be uniformly described and requires systematic case studies. Now, this section investigates the performance of the boost converter with current mode control.

Figure 1.19 is the circuit diagram of the current mode-controlled boost converter. The power stage parameters and operational conditions are the same as those of

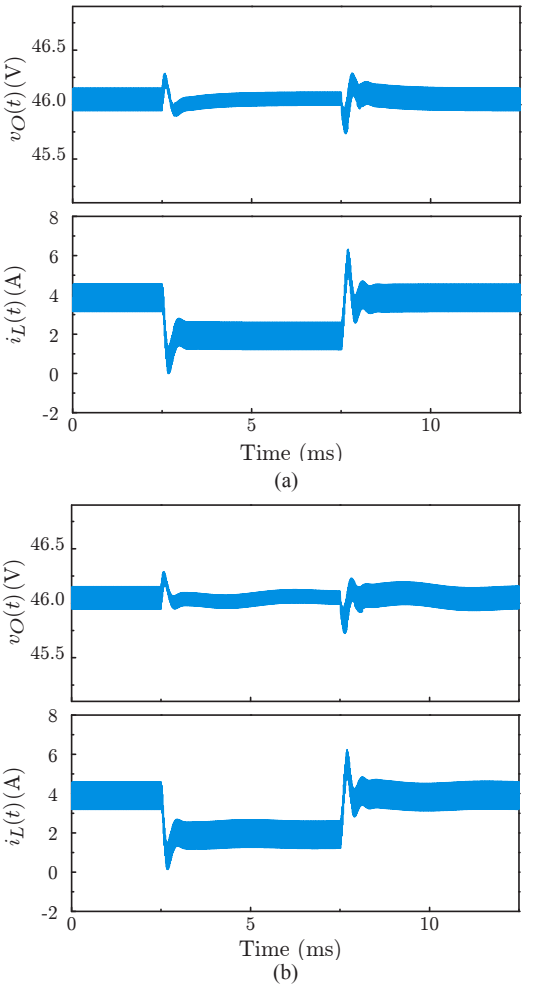

Figure 1.18 Step load response of boost converter. (a) Uncoupled converter. (b) Input filter-coupled converter.

the previous voltage mode-controlled boost converter. For current mode control, the current sensing network (CSN) gain is selected $R_i = 0.45$ and the slope of the compensation ramp is chosen $S_e = 3.9 \times 10^4$ V/sec. The two-pole one-zero circuit

$$F_v(s) = \frac{Z_2(s)}{Z_1(s)} = \frac{6.2 \times 10^3}{s} \frac{\left(1 + \dfrac{s}{2\pi \cdot 263}\right)}{\left(1 + \dfrac{s}{2\pi \cdot 6.21 \times 10^3}\right)}$$

is used for the voltage feedback compensation.

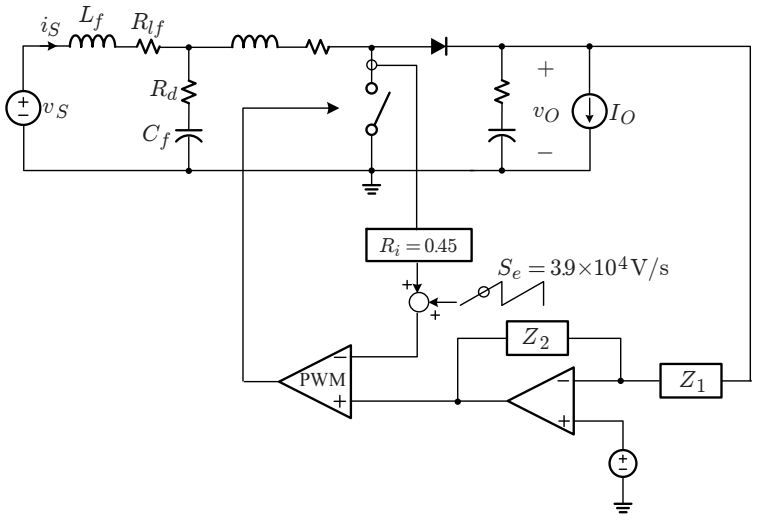

Figure 1.19 Input filter-coupled boost converter with current mode control.

The analysis method used for voltage mode control will be applied to the boost converter with current mode control. The equations for the converter performance are the same. However, the input impedances of the converter are substantially altered, producing very different results. This section starts with the discussions about the input impedances of the boost converter with current mode control.

1.3.1 Input Impedance Analysis

The input impedances with current mode control can be studied in the same manner as that of the previous section. However, the derivations are rather lengthy and complex due to the internal feedbacks associated with current mode control. A reference paper [8] provided a comprehensive input impedance analysis for the three basic converters employing either voltage mode control or current mode control. The outcomes of this paper are summarized in Table 1.1 at the end of this section.

Referring to Table 1.1, the theoretical input impedances of the boost converter with current mode control are shown in Fig. 1.20(a). Figure 1.20(b) displays the simulated input impedances of the boost converter with the given operational conditions.

The input impedances significantly differ from the case of voltage mode control. The open-loop input impedances, $Z_i'(s)$ and $Z_i'''(s)$, are well damped by the internal feedbacks created by current mode control, yielding a flat mid-frequency asymptote. At low and mid frequencies, $|Z_i'|$ and $|Z_i'''|$ are substantially increased so that the condition $|Z_{iU}| \approx |Z_i''| \ll |Z_i'| \approx |Z_i'''|$ prevails. The closed-loop input impedances, $Z_{iU}(s)$ and $Z_i''(s)$, behave as a negative resistance of $-V_S/I_S$ at the frequencies below the loop gain crossover, as is the case with voltage mode control.

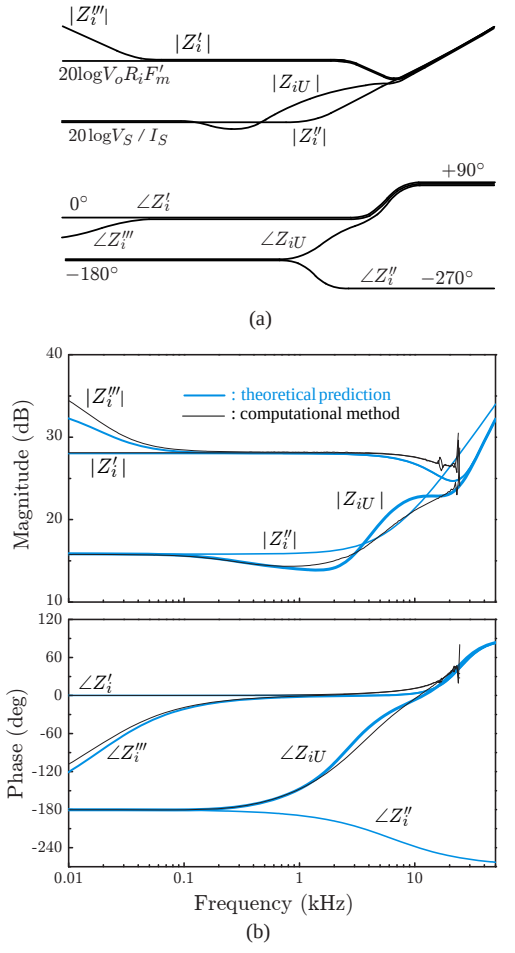

Figure 1.20 Input impedances of boost converter. (a) Asymptotic plot. (b) Input impedances of boost converter with given parameters.

Based on the input impedance characteristics, the following conclusions regarding the input filter interaction can be drawn.

1) The stability condition $|Z_{of0}|_{peak} < V_S/I_S$ should be met for any practical converters. This stability requirement guarantees the conditions $|Z_{of0}/Z_i'| \ll 1$ and $|Z_{of0}/Z_i'''| \ll 1$ with the input impedance characteristics in Fig. 1.20.

   The audio-susceptibility is given by

$$A_{uS}(s) = A_{uf}(s)A_{uU}(s)\,\frac{1}{1+\dfrac{Z_{of0}}{Z_{iU}(s)}} \tag{1.29}$$

The output impedance is simplified into an approximation

$$Z_{oS}(s) = Z_{oU}(s)\,\frac{1+\dfrac{Z_{of0}}{Z_i'(s)}}{1+\dfrac{Z_{of0}}{Z_{iU}(s)}} \approx \boxed{Z_{oU}(s)\,\frac{1}{1+\dfrac{Z_{of0}}{Z_{iU}(s)}}} \tag{1.30}$$

with the condition $|Z_{of0}/Z_i'| \ll 1$.

Finally, the loop gain is expressed as

$$T_{mS}(s) = T_{mU}(s)\,\frac{1+\dfrac{Z_{of0}}{Z_i''(s)}}{1+\dfrac{Z_{of0}}{Z_i'''(s)}} \approx \boxed{T_{mU}(s)\left(1+\frac{Z_{of0}}{Z_i''(s)}\right)} \tag{1.31}$$

due to the condition $|Z_{of0}/Z_i'''| \ll 1$.

In the expressions (1.29) through (1.31), the terms $1/(1+Z_{of0}/Z_{iU}(s))$ and $1+Z_{of0}/Z_i''(s)$ appear as a multiplication factor that carries the impacts of the input filter. When $|Z_{of0}|_{peak}$ is less than V_S/I_S but nears $|Z_{iU}|$ or $|Z_i''|$ in the frequency range where $\angle Z_{iU} \approx \angle Z_i'' \approx -180°$, the multiplication factors $1/\left(1+Z_{of0}/Z_{iU}(s)\right)$ and $1+Z_{of0}/Z_i''(s)$ become infinitely large or vanishingly small. The resulting multiplication factors will exert a strong influence on the performance criteria that contain these multiplication factors in their expression. For example, the loop gain of the converter

$$T_{mS}(s) \approx T_{mU}(s)\left(1+\frac{Z_{of0}}{Z_i''(s)}\right)$$

will be affected as follows. When $|Z_{of0}|_{peak}$ nears $|Z_i''|$ at frequencies where $\angle Z_i'' \approx -180°$, the impedance ratio $Z_{of0}/Z_i''(s)$ approaches -1, because $|Z_{of0}| \approx |Z_i''|$ with $\angle Z_{of0} = 0°$ and $\angle Z_i'' = -180°$ at the frequencies of the $|Z_{of0}|$ peaking. Then, the multiplication factor $1+Z_{of0}/Z_i''(s)$ becomes very small. This in turn causes a drop in $|T_{mS}|$ at frequencies where$|Z_{of0}|_{peak}$ occurs.

2) When $|Z_{of0}|$ is sufficiently reduced to meet $|Z_{of0}|_{peak} \ll 20\log(V_S/I_S)$, all the conditions for the minimal input filter interaction are satisfied: $|Z_{of0}/Z_{iU}| \ll 1$, $|Z_{of0}/Z_i'| \ll 1$, $|Z_{of0}/Z_i''| \ll 1$, and $|Z_{of0}/Z_i'''| \ll 1$. Under this condition, the influence of the input filter is negligible and the converter performance reduces to the performance of the uncoupled converter: $A_{uS}(s) \approx A_{uf}(s)A_{uU}(s)$, $Z_{oS}(s) \approx Z_{oU}(s)$, and $T_{mS}(s) \approx T_{mU}(s)$.

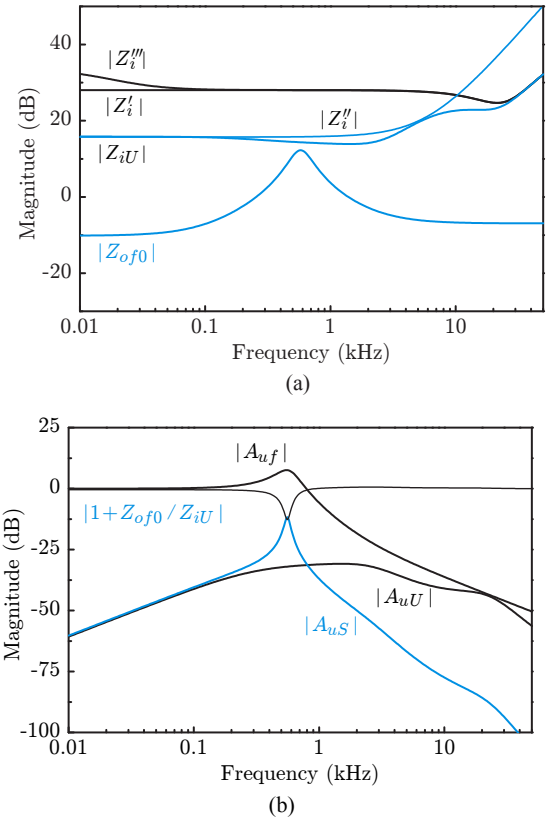

Figure 1.21 Transfer functions of boost converter with current mode control. (a) Converter input impedances and input filter output impedance. (b) Audio-susceptibility.

1.3.2 Converter Performance under Input Filter Interaction

This section investigates the performance of the converter with a specific input filter which barely meet the stability requirement of $|Z_{of0}|_{peak} \ll 20\log(V_S/I_S)$. The input filter is designed as $L_f = 2200\ \mu$H, $R_{lf} = 0.19\ \Omega$, $C_f = 1200\ \mu$F, $R_{cf} = 0.057\ \Omega$, in order to push $|Z_{of0}|_{peak}$ very close to $|Z_{iU}|$ and $|Z_i''|$, but smaller than $20\log(V_S/I_S)$.

Figure 1.21(a) shows the output impedance of the input filter, together with the input impedances of the boost converter. The conditions of $|Z_{of0}|_{peak} \ll |Z_i'|$ and $|Z_{of0}|_{peak} \ll |Z_i'''|$ are well met, but $|Z_{of0}|_{peak}$ approaches $|Z_{iU}|$ and $|Z_i''|$ at the frequency where $\angle Z_i'' \approx \angle Z_{iU} \approx -180°$. The audio-susceptibility $A_{uS}(s)$ is shown in Fig. 1.21(b), along with the transfer functions involved with the formation of $A_{uS}(s)$. As predicted, the condition $|Z_{of0}|_{peak} \approx |Z_{iU}|$ induces a dipping to

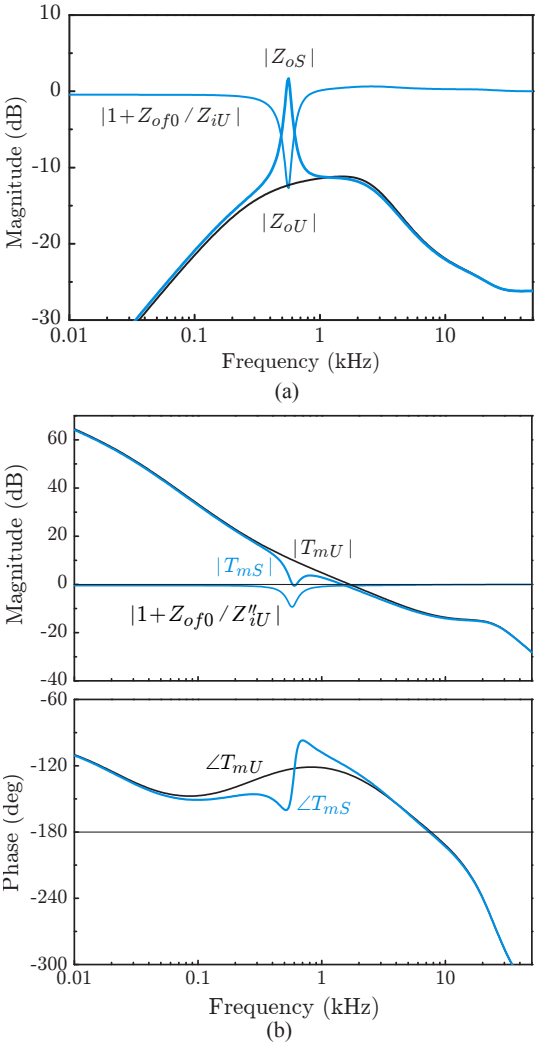

Figure 1.22 Transfer functions of boost converter with current mode control. (a) Output impedance. (b) Loop gain.

the multiplication factor $1 + Z_{of0}/Z_{iU}(s)$, which in turn incurs a peaking in the audio-susceptibility

Figure 1.22(a) illustrates the formation of the output impedance. Similar to the audio-susceptibility case, the nearness of $|Z_{of0}|_{peak}$ to $|Z_{iU}|$ yields a drop in $1 + Z_{of0}/Z_{iU}(s)$, producing an upsurge in the output impedance $Z_{oS}(s)$.

The loop gain of the converter is displayed in Fig. 1.22(b). Due to the closeness between $|Z_{of0}|_{peak}$ and $|Z_i''|$, the loop gain experiences a dip, causing a premature

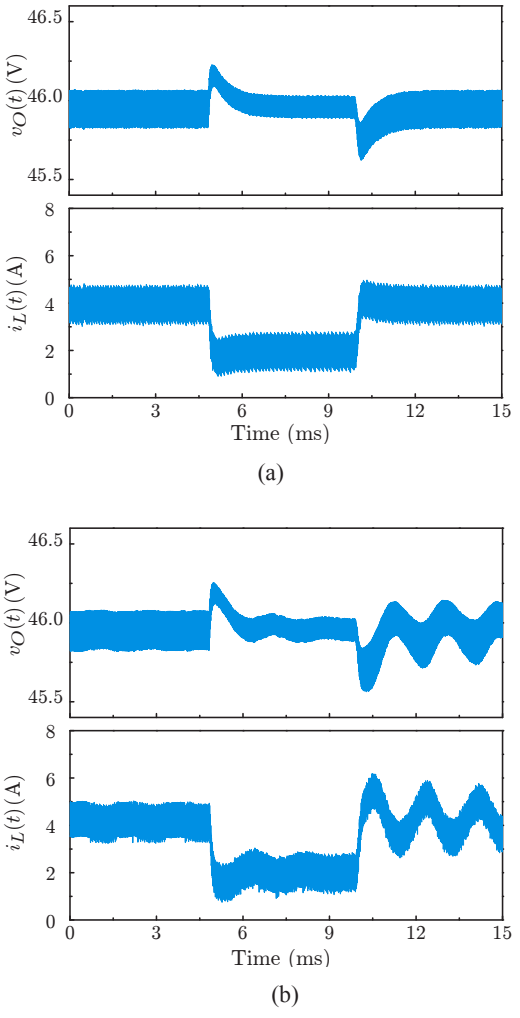

Figure 1.23 Step load response of boost converter with current mode control. (a) Uncoupled boost converter. (b) Input filter-coupled boost converter

0 dB crossover with a marginal phase margin. The loop gain clearly indicates that the converter is on the brink of instability.

Lastly, Fig. 1.23 depicts the transient responses of the input filter-coupled converter and uncoupled converter. The transient responses are generated with the step load changes of $I_O = 2\ \text{A} \Rightarrow 1\ \text{A} \Rightarrow 2\text{A}$. While the uncoupled converter shows a very stable behavior, the boost converter combined with the input filter exhibits nearly unstable response.

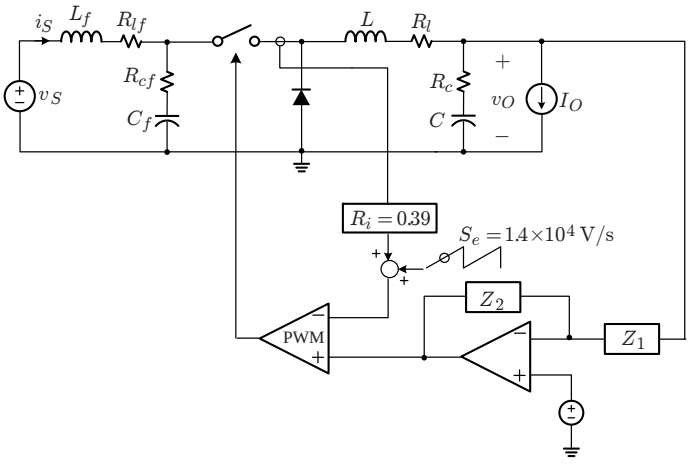

Figure 1.24 Input filter-coupled buck converter with current mode control.

1.3.3 Conditions for Minimal Input Filter Interaction

Referring to Fig. 1.20, the impedance constraint for the minimal input filter interaction is now simplified to one condition $|Z_{of0}|_{peak} \ll 20\log(V_S/I_S)$. This condition guarantees that $|Z_{of0}/Z_{iU}| \ll 1$, $|Z_{of0}/Z_i'| \ll 1$, $|Z_{of0}/Z_i''| \ll 1$, and $|Z_{of0}/Z_i'''| \ll 1$ and ensures all the performance of the converter unaffected by the input filter. Current mode control thus eases the input filter design, compared with the voltage mode control.

1.4 INPUT FILTER INTERACTION CASE THREE – BUCK CONVERTER WITH CURRENT MODE CONTROL

We demonstrated that current mode control markedly alters the outcomes of the input filter interaction. In this section, we will study a more interesting phenomenon, taking place when current mode control is employed to the buck converter. Most significantly, the impacts of the input filter are *unobservable* in the loop gain and output impedance of the converter. In other words, the loop gain and output impedance are essentially unaffected by the input filter that pushes the converter to the boundary of stable operation or even well into the unstable region. This eccentric behavior puzzled many researchers and has been a subject of disputes and clarifications. This section addresses the impacts of input filter, aiming to uncover the theory behind the aforementioned peculiarity of the current-mode controlled buck converter.

Figure 1.24 is the circuit diagram of the buck converter used for input filter interaction analysis. The operational conditions of the converter are $V_S = 46$ V, $V_O = 15$ V, $I_O = 3$ A, $L = 180$ μH, $R_l = 0.12$ Ω, $C = 400$ μF, $R_c = 0.035$ Ω, and $f_s = 50$ kHz. The parameters for current mode control are $R_i = 0.39$ and

$S_e = 1.4 \times 10^4$ V/sec. The two-pole one-zero circuit

$$F_v(s) = \frac{Z_2(s)}{Z_1(s)} = \frac{1 \times 10^4}{s} \frac{\left(1 + \dfrac{s}{2\pi \cdot 367}\right)}{\left(1 + \dfrac{s}{2\pi \cdot 1.07 \times 10^4}\right)}$$

is used for the voltage feedback compensation.

The same as the previous cases, the input impedances of the converter play the central role in the input filter interaction. Now, we investigate the input impedances of the buck converter.

1.4.1 Input Impedance Analysis

Figure 1.25(a) depicts the input impedances of the buck converter with current mode control. The asymptotic impedance plots are cited from Table 1.1 at the end of this section. Very interestingly, the four input impedances altogether have the same magnitude of $20\log(V_S/I_S)$ and the same phase of $-180°$ from dc to mid frequencies. This implies that the four input impedances all become the negative resistance of $-V_S/I_S$, $Z_{iU}(s) \approx Z_i'(s) \approx Z_i''(s) \approx Z_i'''(s) \approx -V_S/I_S$, for the frequencies of practical importance. This unique feature of the buck converter is the consequential outcome of the internal feedbacks involved with current mode control [9].

The input impedances of the buck converter for the given operational conditions are shown in Fig. 1.25(b). As predicted from the asymptotic plots, all the four input impedances indeed behave as a negative resistance of $-V_S/I_S$ for a wide frequency range. This distinctive characteristics yield the very unique input filter interaction.

1.4.2 Converter Performance under Input Filter Interaction

This section investigates the performance of the current-mode controlled buck converter coupled with the following three different input filters.

- Filter A: $L_f = 21\ \mu$H, $R_{lf} = 0.04\ \Omega$, $C_f = 160\ \mu$F, $R_{cf} = 0.037\ \Omega$
- Filter B: $L_f = 140\ \mu$H, $R_{lf} = 0.05\ \Omega$, $C_f = 180\ \mu$F, $R_{cf} = 0.18\ \Omega$
- Filter C: $L_f = 610\ \mu$H, $R_{lf} = 0.125\ \Omega$, $C_f = 392\ \mu$F, $R_{cf} = 0.15\ \Omega$

Figure 1.26 shows the input impedances of the buck converter and the output impedance of the input filters. As shown in Fig. 1.26(a), $|Z_{of0}|_{peak}$ of the input filters is successively increased in order to produce an escalating stage of the input filter interaction. Filter A reveals $|Z_{of0}|_{peak} \ll V_S/I_S$ and satisfies the conditions $|Z_{of0}/Z_{iU}| \ll 1$, $|Z_{of0}/Z_i'| \ll 1$, $|Z_{of0}/Z_i''| \ll 1$, and $|Z_{of0}/Z_i'''| \ll 1$ for the minimal input filter interaction. Thus, the converter will stay stable and its performance will not vary from the uncoupled converter case. For Filter B, the stability requirement of $|Z_{of0}|_{peak} < 20\log(V_S/I_S)$ is met. However, $|Z_{of0}|_{peak}$ is

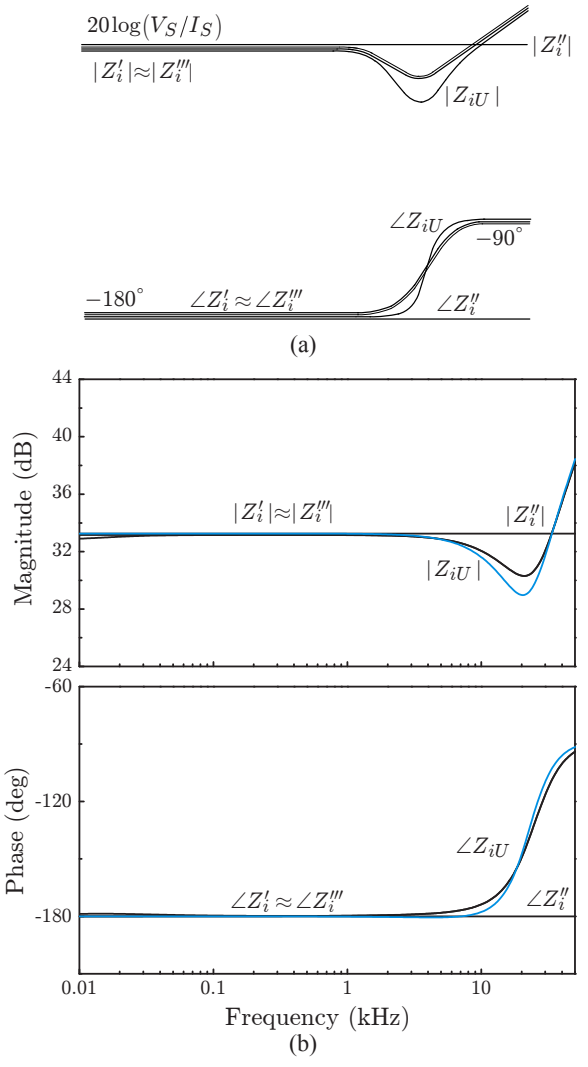

Figure 1.25 Input Impedances of current-mode controlled buck converter. (a) Asymptotic plot. (b) Input impedance of buck converter with given parameters.

not sufficiently separated from the $20\log(V_S/I_S)$ asymptote of the input impedances. Although the converter will be stable, its performance will be adversely affected by the input filter. Lastly, the $|Z_{of0}|_{peak}$ of Filter C rises over $20\log(V_S/I_S)$, thereby pushing the converter into the unstable operation.

Shown in Fig. 1.26(b) are the polar plot trajectories of the impedance ratio of $Z_{of0}/Z_{iU}(s)$. The polar plot predictions are consistent with the previous stability assessment. Filter A well satisfies the Nyquist criterion. On the other hand, Filter

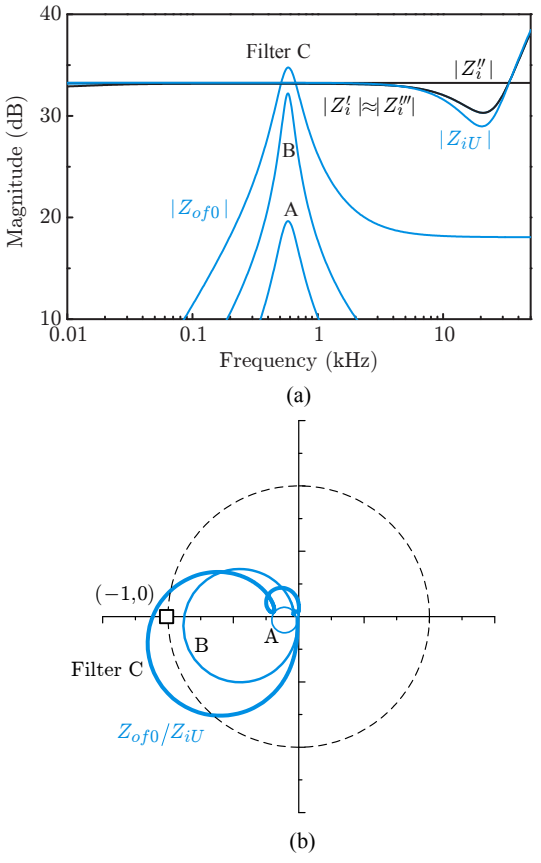

Figure 1.26 Output impedances of filters and input impedances of converter. (a) Bode plot of impedances. (b) Polar plots of impedance ratio Z_{of0}/Z_{iU}.

B barely meets the stability criterion with very small margin, while Filter C violates the stability requirement.

Figure 1.27 illustrates the closed-loop performance of the converter coupled with the three input filters. Impacts of the filters on the audio-susceptibility are shown in Fig. 1.27(a). The audio-susceptibility explicitly shows the consequence of the input filter interaction. The audio-susceptibility is given by

$$A_{uS}(s) = A_{uf}(s)A_{uU}(s)\,\frac{1}{1+\dfrac{Z_{of0}}{Z_{iU}(s)}} \tag{1.32}$$

Filter A offers a comfortable distance between $|Z_{of0}|_{peak}$ and $|Z_{iU}|$. When $|Z_{of0}|_{peak}$ approaches $|Z_{iU}|$ with Filter B, the magnitude of the multiplication factor $1/(1 + Z_{of0}/Z_{iU}(s))$ becomes larger, thereby causing a peaking in $|A_{uS}|$ and an abrupt $180°$

drop in $\angle A_{uS}$. This signifies the presence of an underdamped left-half plane (LHP) double pole. The LHP double pole crosses the imaginary axis to become an unstable right-half plane (RHP) double pole when $|Z_{of0}|_{peak}$ rises above $20\log(V_S/I_S)$. This instability occurred with Filter C, where $\angle A_{uS}$ increased by 180° as shown in Fig. 1.27(a). The audio-susceptibility fully exposes the internal status of the converter with the different input filters. However, the situation is utterly different when the other performance criteria are concerned.

The input impedance analysis confirmed that $Z_{iU}(s)$ and $Z_i'(s)$ are practically the same. The output impedance contains the ratios of $Z_{of0}/Z_{iU}(s)$ and $Z_{of0}/Z_i'(s)$ in its expression, one in the denominator and the other in the numerator. Thus, the output impedance will remain unchanged from the output impedance of the uncoupled converter, due to the canceling of the two multiplication factors.

$$Z_{oS}(s) = Z_{oU}(s)\,\frac{1+\dfrac{Z_{of0}}{Z_i'(s)}}{1+\dfrac{Z_{of0}}{Z_{iU}(s)}} \approx Z_{oU}(s) \tag{1.33}$$

This indicates that the effects of the input filter are totally hidden and the output impedance always stays the same, regardless of any changes in stability and other internal dynamics of the converter. The output impedance plots in Fig. 1.27(b) verifies this fact.

The phenomenon found in the output impedance also happens in the loop gain in Fig. 1.27(c). With the prevailing condition of $Z_i''(s) \approx Z_i'''(s)$, the loop gain becomes

$$T_{mS}(s) = T_{mU}(s)\,\frac{1+\dfrac{Z_{of0}}{Z_i''(s)}}{1+\dfrac{Z_{of0}}{Z_i'''(s)}} \approx T_{mU}(s) \tag{1.34}$$

The loop gain is unaltered and does not show any abnormality when the converter is at the borderline of stability or even in deep instability. This situation is the same as the output impedance case.

The step load current response of the buck converter is shown in Fig. 1.28. The output voltage in response to the load current changes of $I_O = 2\text{ A} \Rightarrow 1\text{ A} \Rightarrow 2\text{ A}$ is displayed. Filter A produces the same transient response as that of the uncoupled converter. With Filter B, the output voltage shows a nearly unstable response, as predicted from the small-signal analysis. The converter exhibits a full oscillation with the unstable Filter C.

As demonstrated in this section, the input filter interaction is totally unobservable in the loop gain and output impedance of the converter. The stability should not be judged from the loop gain. The step load response can not be estimated from the output impedance. The correct information about the stability and internal dynamics is solely available from the impedance ratio of $Z_{of0}/Z_{iU}(s)$ and the audio-susceptibility. This is a very intriguing phenomenon, only existing in current-mode controlled buck converters.

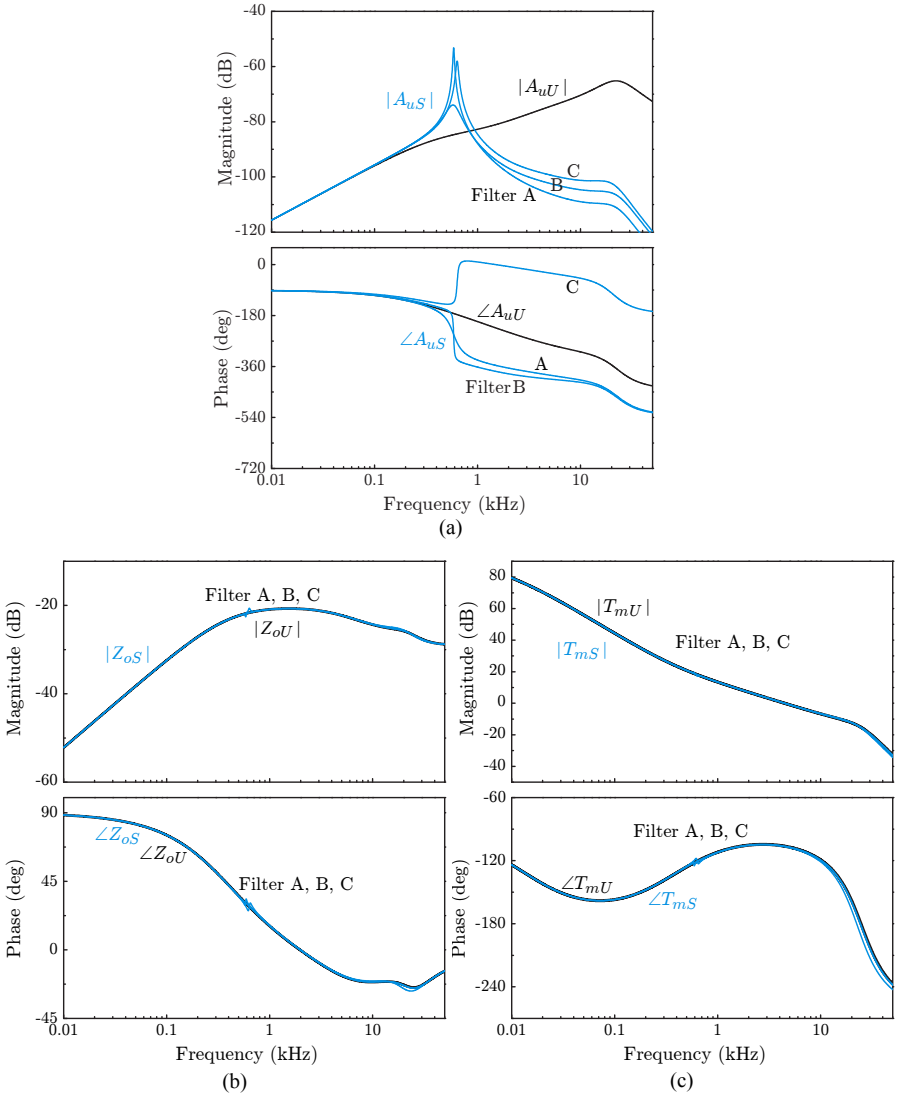

Figure 1.27 Closed-loop performance. (a) Audio-susceptibility. (b) Output impedance. (c) Loop gain.

1.5 CHAPTER SUMMARY

In this chapter, we investigated the small-signal dynamics of input filter-coupled converters. Details about the input filter interaction are all addressed using the three converter examples. We first established the conditions to secure the stability and

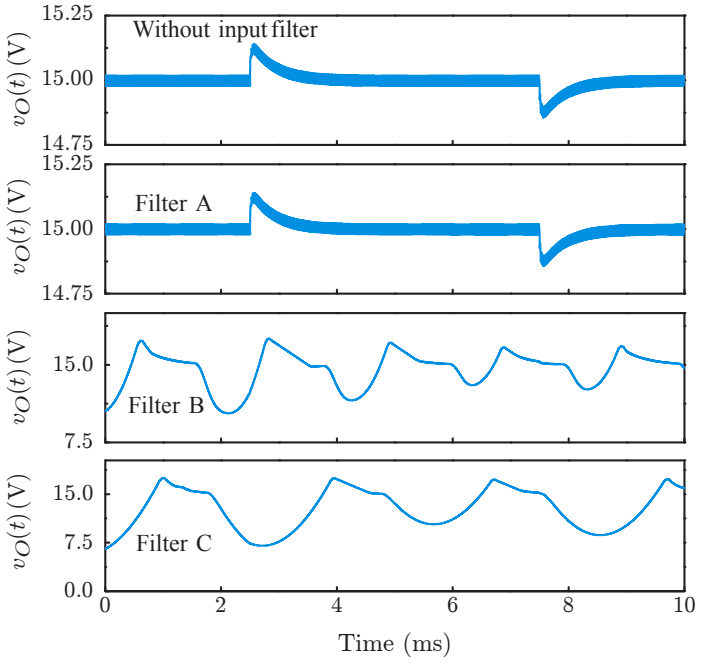

Figure 1.28 Step load response with different filters.

minimal performance change for converters. Later, we analyzed the closed-loop performance of the converters under strong influences of the input filter interaction.

The impacts of the input filter are determined by the relative magnitudes of the output impedance of the input filter and the input impedance of the converter. Here, the four different input impedances of the converter are needed to completely describe the effects of the input filter. The circuit representations of the four input impedances were given in Fig. 1.4.

Table 1.1 shows the Bode plots of the four different input impedances of the three basic converters with two different control schemes. Referring to the input impedance characteristics in Table 1.1, the outcomes of this chapter are summarized.

Condition for Stability

The input filter-coupled converters remain stable if the peak value of the output impedance of the input filter, $|Z_{of0}|_{peak}$ does not exceed the low-frequency asymptote of the closed-loop input impedance of the converter, $|Z_{iU}(0)|$. As verified in Section 7.2.1 and shown in Table 1.1, the low-frequency asymptote of $Z_{iU}(s)$ is determined as $|Z_{iU}(0)| = 20\log(V_S/I_S)$ for all the converters. Thus, the stability requirement

Table 1.1 Input Impedances of Three Basic Converters

Voltage mode control	Current mode control
Buck converter	
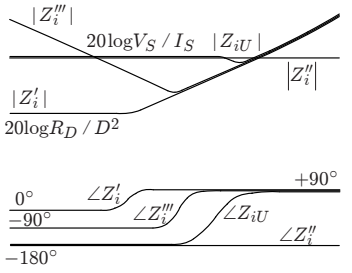	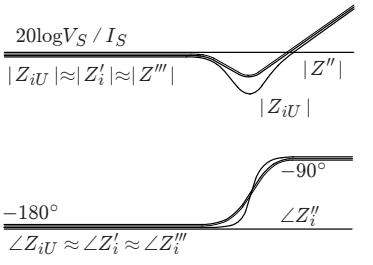
Boost converter	
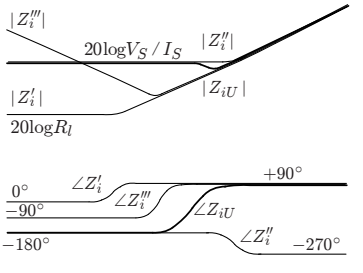	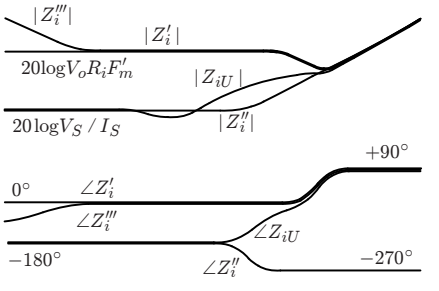
Buck/boost converter	
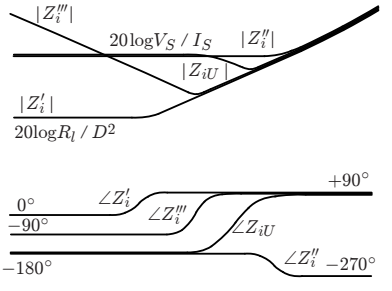	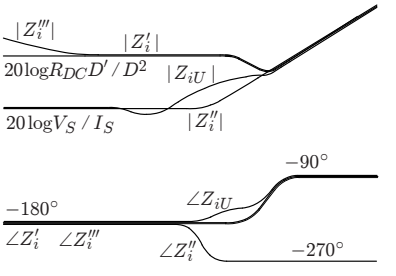

of all the input filter-coupled converters is given by

$$|Z_{of0}|_{peak} < 20\log\left(\frac{V_S}{I_S}\right) \tag{1.35}$$

regardless of the converter topology and control scheme. A more conservative requirement of $|Z_{of0}|_{peak} \ll 20\log(V_S/I_S)$ is often employed in considerations of potential changes and tolerance in the operational conditions of the converter.

Conditions for Minimal Performance Change

We identified the three conditions to prevent the converter from being affected by the input filter.

1) $|Z_{of0}|_{peak} \ll 20\log(V_S/I_S)$

2) $|Z_{of0}|_{peak} \ll |Z_i'|$ where $Z_i'(s)$ is the open-loop output-shorted input impedance of the converter.

3) $|Z_{of0}|_{peak} \ll |Z_i'''|$ where $Z_i'''(s)$ is the open-loop input impedance of the converter.

The first condition is the same as the conservative requirement for stability. For current-mode controlled converters, the condition 1) automatically includes the other two conditions of 2) and 3) for the reason explained below. As shown in Table 1.1, $|Z_i'| \gg 20\log(V_S/I_S)$ and $|Z_i'''| \gg 20\log(V_S/I_S)$ for the current-mode controlled boost and buck/boost converters and $|Z_i'| \approx |Z_i'''| \approx 20\log(V_S/I_S)$ for the current-mode controlled buck converter. Thus, the conservative stability requirement $|Z_{of0}|_{peak} \ll 20\log(V_S/I_S)$ also ensures the minimal performance change for all the current-mode controlled dc-to-dc converters.

The situation is quite different for voltage-mode controlled dc-to-dc converters, in which the condition $|Z_i'| \ll |Z_i'''| \ll 20\log(V_S/I_S)$ prevails as shown in Table 1.1. Under this condition, it is impractical to meet all the three conditions for the total elimination of the input filter interaction. For most cases, the stability condition $|Z_{of0}|_{peak} \ll 20\log(V_S/I_S)$ can be met but $|Z_{of0}|$ partially exceeds $|Z_i'|$ or $|Z_i'''|$, thus violating the conditions of 2) and 3). As a consequence, the loop gain and output impedance will be modified by the input filter. Nonetheless, it was demonstrated that the modifications do not necessarily worsen the converter performance and are usually acceptable in practice.

Converter Performance under Input Filter Interaction

We also analyzed the performance of the converters under strong influences of the input filter interaction. The converter performance is described by the same set of equations for all the dc-to-dc converters. Even so, the end results of the input filter interaction emerge very differently and uniquely, depending on the converter topology and control scheme. The evolution of the input filter interaction is dictated by the shape and pattern of various input impedances of the converter. Referring to Table 1.1, the input impedances can be classified into the following three cases. Each case generates the distinctive outcomes of the input filter interaction.

Voltage-mode controlled three basic converters When voltage mode control is employed, the input impedances of the three basic converters are largely the same. Thus, the evolution of the input filter interaction will be similar. The input filter interaction for this case was investigated in Section 7.2 using the boost converter example. When the input filter is duly designed, the converter will remain stable. However, the loop gain and output impedance will be affected by the input filter. Nev-

ertheless, the changes won't degrade the frequency- and time-domain performance of the converter, as demonstrated in Figs. 1.17 and 1.18. The results of this section can be extended to all the three basic converters as far as voltage mode control is adapted.

Current-mode controlled boost and buck/boost converters When current mode control is employed, the input impedances of the converter significantly vary from the case of voltage mode control. In particular, the current feedback provides an effective damping for the open-loop input impedances of the converter, thereby notably enhancing their magnitude. Very importantly, the consequences of this change develop in a similar format for the boost and buck/boost converters, but in a much dissimilar form for the buck converter, as demonstrated in Table 1.1. Section 7.3 covered the cases of the boost and buck/boost converters using using the boost converter example.

For boost and buck/boost converter cases, stability will be maintained if $|Z_{of0}|_{peak}$ does not exceed $20\log(V_S/I_S)$. However, as $|Z_{of0}|_{peak}$ moves closer to $20\log(V_S/I_S)$, the performance will be increasingly deteriorated. The audio-susceptibility and output impedance show a growing peaking. The phase margin of the loop gain will be successively lessened and transient responses will become more oscillatory, as shown in Figs. 1.21 through 1.23.

Current-mode controlled buck converter As shown in Table 1.1, the magnitudes of the four input impedances of the current-mode controlled buck converter all merge together to the same value of $20\log(V_S/I_S)$. This unique property results in the very distinctive input filter interaction.

Similar to the boost converter and buck/boost converter cases, the performance mainly remains unchanged if the condition $|Z_{of0}|_{peak} \ll 20\log(V_S/I_S)$ is met. When $|Z_{of0}|_{peak}$ increase towards $20\log(V_S/I_S)$, the converter moves to the borderline of stability and becomes unstable with the condition $|Z_{of0}|_{peak} > 20\log(V_S/I_S)$. Nevertheless, these crucial changes are totally undetectable in the loop gain and output impedance. The *same magnitude* of the four input impedances hides any changes in the converter dynamics. Consequently, the loop gain and output impedance appear the same without any sign of abnormality or improperness, even for the converter in deep instability. For this case, only the impedance ratio of $Z_{of0}/Z_{iU}(s)$ and audio-susceptibility carry the correct information about the stability and performance of the converter. Section 7.4 dealt with this eccentric case of the input filter interaction.

Extension to General Source-Coupled Converters

The input filter interaction analysis can be directly extended to general source subsystems as far as the the output impedance of the source subsystem is available. All the equations of the input filter-coupled converters are valid for the converters coupled with general source subsystems. Extensions of the outcomes of this chapter to converters in dc power conversion systems will be covered in Part III of this book.

REFERENCES

1. R. D. Middlebrook, "Null double injection and the extra element theorem," *IEEE Trans. Ed.* vol. 32, no. 3, pp.167-180, Aug. 1989.
2. R. D. Middlebrook, V. Vorpérion, and J. Lindel, "The N extra element theorem," *IEEE Trans. Circuit Syst. I,* vol. 45, no. 9, pp.919-935, Sep. 1998.
3. V. Vorpérion, *Fast Analytical Techniques for Electrical and Electronic Circuits,* Cambridge University Press, 2002.
4. B. Choi, D. Kim, D. Lee, S. Choi, and J. Sun, "Analysis of input filter interaction in switching power converters," *IEEE Trans. Power Electron.,* vol. 22, no. 2 pp. 452-459, Oct. 1999.
5. D. Kim, B. Choi, D. Lee, and J. Sun, "Dynamics of current-mode-controlled dc-to-dc converters with input filter stage," in *PESC Conf. Rec.,* 2005.
6. D. Lee, B. Choi, J. Cho, and B. Cho, "Interpretation and prediction of loop gain characteristics for switching power converters loaded with general load subsystem," in *PESC Conf. Rec.,* 2005.
7. D. Kim, D. Son, and B. Choi, "Input impedance analysis of PWM dc-to-dc converters," in *APEC Conf. Rec.,* 2006.